Adjusting the Morphology and Properties of SiC Nanowires by the Catalyst Control

Chuchu Guo
Northwestern Polytechnical University
Laifei Cheng (chenglf@nwpu.edu.cn)
Northwestern Polytechnical University
Fang Ye (yefang511@nwpu.edu.cn)
Northwestern Polytechnical University

Research Article

Keywords: Silicon carbide nanowires, vapor-solid-liquid mechanism, oxide-assisted growth mechanism, photoluminescence, thermal stability

Posted Date: June 8th, 2020

DOI: https://doi.org/10.21203/rs.3.rs-33288/v1

Abstract

Herein, we report the growth of SiC nanowires on a single crystal Si substrate by pyrolysis of polycarbosilane and using two catalyst (Al_2O_3 and Ni) films with different thickness (2, 4, and 6 nm). The catalyst films were deposited on the Si substrate, and the SiC nanowires were grown according to two mechanisms, i.e., the oxide-assisted growth mechanism and vapor- liquid-solid mechanism. As a result, the pearl-chain-like SiC nanowires and straight SiC nanowires were obtained. The prepared nanowires exhibited excellent photoluminescence properties, the emission spectra displaying two emission peaks at 395 and 465 nm, and have good thermal stability below 1000℃.The experimental results revealed the importance of the catalyst in controlling the morphology and properties of SiC nanowires.

1. Introduction

In the nanometer scale, the surface effect, small size effect, quantum size effect and macroscopic tunneling effect dramatically change the physical and chemical properties of materials[1–3]. For instance, SiC nanowires, a non-oxide ceramic material, attracted a high interest as a highly promising nanomaterial for many industrial applications due to the superior electric and mechanical properties, as well as heat, corrosion, and high temperature oxidation resistance[4]. These unique properties enable SiC nanowires to be used as ideal candidates for nanodevices for sensing and biosensing applications, or in composite materials as an reinforcement[5]. To the key role, SiC nanowires widely used in aerospace, nuclear, braking systems and other industrial fields[6–8]. The development of high-performance materials and the maturity of preparation technology have stimulated the researchers to design and create the SiC nanowires with higher performance, which further promoted deeper research on the growth mechanism of SiC nanowires.

Oxides are commonly used as catalysts to grow nanowires through the oxide-assisted growth (OAG) mechanism, whereas transition metals are often used as catalysts for the growth of nanomaterials by the vapor-liquid-solid (VLS) mechanism. Zhang[9] studied the growth of Si nanowires with uniform size and long length by OAG and VLS mechanisms, aiming at achieving a controlled growth of nanowires. Kang[10] used Au catalyst to prepare III-V semiconductor nanowires with a certain angle and extended (111) direction on the (001) Si substrate by VLS mechanism. Zhang[11] prepared bamboo-like SiC nanowires by doping Al catalyst during the pyrolysis of polycarbosilane (PCS). The findings highlighted the positive role played by the catalyst during the growth of semiconductor and oxide nanowires. Nevertheless, only few reports on the growth of SiC nanowires in the presence of catalysts and different growth mechanisms are available in the literature.

This work is focused on the preparation of SiC nanowires, displaying different morphologies, by changing the type and content of catalyst loaded on the substrate. The nanowires were grown on the single crystal silicon substrate by VLS and OAG mechanisms. The phase composition, microstructure, and morphology, as well as the photoluminescence properties and thermal stability of the prepared SiC nanowires were

analyzed. The growth mechanisms of SiC nanowires were described in detail, providing fundamental knowledge for the rational control of the morphology of SiC nanowires.

2. Experimental

2.1 Synthesis of samples

30 g of polycarbosilane (PCS) precursor (Xiamen University) was dissolved under magnetic stirring for 30 min. The catalyst film (Al_2O_3 or Ni) with 2, 4, and 6 nm thickness was deposited on a single crystal Si substrate by ion beam-assisted deposition. The precursor was then poured into a crucible, which was transferred in a tube furnace. The substrate with catalyst film was placed downstream 5 cm from the precursor. The air in the furnace was replaced with Ar gas at a flow rate of 40 SCCM. The temperature was raised to 1350 °C at a rate of 5 °C/min and held for 3 h. The obtained products were named as A1, A2, A3, respectively for the samples prepared with Al_2O_3 catalyst film at a thickness of 2, 4, and 6 nm, and N1, N2, N3, respectively for the samples prepared with Ni catalyst film at a thickness of 2, 4, and 6 nm..

2.2 Characterization of samples

The obtained SiC nanowires were coated with a 5 nm layer of gold for scanning electron microscopy (SEM) imaging. The images were taken using a field emission scanning electron microscope (FE-SEM, S-4700). Samples were also observed by transmission electron microscopy (TEM) using a FEI Talos F200X microscope. Crystal phases were characterized by an X-ray diffractometer (X-ray diffraction, XRD, AXS D8). The photoluminescence properties were characterized by X-ray fluorescence spectrometry (Axios-X), and the thermal stability of the samples was measured with TG-DSC equipment at 10 ° C/min to 1400 ° C air atmosphere (GCMS QP2010 PLUS).

3. Results And Discussion

The morphology and growth mechanism of SiC nanowires were controlled by using different catalysts. The corresponding surface and cross-section morphology SEM images of all six samples are illustrated in Fig. 1 and Fig. 2.

As shown in Fig. 1(a), when the thickness of the Al_2O_3 catalyst is 2 nm, a large number of pearl-like beads are formed on the surface of the substrate, which are in an intimate contact with the surface (Fig. 1(d)). As the thickness of the catalyst film increases, SiC nanowires begin to form, but they are straight and co-exist with the pearl-chain-like nanowires (Fig. 1(b), (c)). Also, the thickness of the nanowire on the substrate surface becomes larger which obviously increased from 11 to 85 μm for the samples prepared with the Al_2O_3 film thickness of 4 and 6 nm, respectively (Fig. 1(e), (f)). The diameter of the straight nanowire is about 50 nm. The minimum diameter of the pearl-chain-like nanowire is about 100 nm, and the maximum diameter of the pearls is about 850 nm. The SEM images of the samples prepared with Ni catalyst are illustrated in Fig. 2. As observed, the diameter of the SiC nanowires catalyzed by Ni film is about 50 nm while their surface is smooth and clean (Fig. 2(a)-(c)). The cross-section image (Fig. 2(d))

shows a mats-like arrangement of the nanowires on the substrate. As the thickness of the Ni catalyst increases to 4 and 6 nm, the thickness of nanowires increases from 63 to 92 μm, respectively, while the layer of nanowires is denser (Fig. 2(e), (f)). These results indicate that different growth mechanisms of the nanowires in the presence of the two catalysts. For A1, A2, and A3 samples, the nanowires are grown following the OAG mechanism. In this case, the growth of SiC nanowires is assisted by semi-liquid Al_2O_3 when an Si-O-Al amorphous layer is formed on the surface of the nanowires, preventing the lateral growth of the nanowires. By contrary, the growth mechanism of the nanowires in N1, N2, and N3 samples is the VLS mechanism. In this case, the catalyst droplets form at lower temperatures. The catalyst droplet can be used as a template to control the morphology of the SiC nanowire at the top of the nanowire. Secondly, the solid-liquid interface is formed at the top of the nanowires, so that the reactants continue to crystallize at the interface to form nanowires.

Fig. 3 displays the XRD patterns of SiC nanowires grown in the presence of the two different catalysts.

As illustrated in Fig. 3 (a), all three samples showed typical diffraction peaks for 3C-SiC. When the thickness of Al_2O_3 is 2 nm, the characteristic peak strength of SiC is extremely weak. As the thickness of the Al_2O_3 catalyst film increases, the characteristic peaks of SiC gradually become sharp and clearly visible. This indicates that the crystallinity of the nanowires is gradually increasing. In Fig. 3(b), the typical diffraction peaks of SiC are displayed even at the lower thickness of the Ni film. Yet, the peaks become sharper as the thickness of the Ni film increases. To note, for the N3 sample, traces of C can be observed in the XRD pattern. The comparison of the crystallinity of samples reveals that a crystallization degree of 22.3% is obtained for the N3 sample, which is made of grains of 14.3 nm, whereas a crystallinity degree of 35.6% is determined for the A3 sample, consisting of grains of 21.1 nm (Table 1). This result is consistent with the SEM result. The sample with Al2O3 as catalyst has a larger diameter, so the overall crystallinity is higher. This is because the semi-liquid catalyst in the OAG growth mechanism is only attached to the surface of SiC nanowires, and the limiting force on the diameter of nanowires is weaker than that on the tip nanowires droplets in the VLS mechanism.

Table 1
Crystallinity and grain size of SiC nanowires grown on the substrate surface in the presence of Ni or Al_2O_3 as catalysts.

Sample	Crystallinity /%	Grain size /nm
A3	35.6	21.1
N3	22.3	14.3

The microstructure and composition of the A3 sample are analyzed by (HR)TEM, SAED, and elemental mapping. The results are displayed in Fig. 4.

Fig. 4 show representative high-resolution(HR) TEM images of A3 sample. It can be observed that two different morphologies co-exist in the sample, a bead-like morphology as well as a smooth and straight

shaped morphology (Fig. 4(a)). The pearl-like beads of ~ 150 nm in diameter, which are placed alongside the nanowire, are amorphous. The core of the beads is crossed by a straight nanowire with a diameter of 50 nm. The *d*-spacing between two neighboring lattice fringes is 0.25 nm, according to the Fig. 4(b). It can be observed from the selected area electron diffraction pattern (SAED) in the Fig. 4(b) inset, that the crystal diffraction lattice co-exists with a halo, attributed to the amorphous phase. Hence, it can be stated that the core of the pearl-like beads is made of a SiC single crystal while the pearl-like structure is amorphous. From Fig. 4(c), it can be observed that the straight SiC nanowires, having a diameter of 50 nm, are grown in the (111) direction. In addition, twin defects can be observed inside the nanowires. The EDS pattern of pearl-chain-like nanowire clearly shows that the amorphous layer mainly contains Si, O, and Al (Fig. 4(d)). As listed in Table 2, in the Area 1, the amorphous Si-O ratio is close to 1: 2 while a small amount of Al is also detected. The Si-C ratio of Area 2 is close to 1, and the atomic content of oxygen is 2.65%, indicating that the core of the nanowire is composed of 3C-SiC single crystals. The microstructure and composition of the smooth and straight nanowires in A3 are the same as the core of the beads discussed above (Fig. 4(e)).

Table 2
Elemental analysis results of different regions in A3 displayed in Fig. 4(d).

Element	**Si**	**C**	**O**	**Al**
Atomic fraction (%)				
Area 1	29.53	2.06	63.39	5.01
Area 2	52.81	44.54	2.65	–

Since no other metal elements participate to the reactions during the synthesis, but only Al_2O_3, it is evident that the nucleation and growth of the A1, A2, and A3 samples are governed by the OAG mechanism. Figure 5 schematically illustrates the growth of SiC nanowires in the presence of Al_2O_3 catalyst via the OAG mechanism.

In the initial stage of the reaction, the Al_2O_3 film deposited on the Si substrate is strongly bonded to substrate, which limits the agglomeration of catalyst on the substrate surface. The pyrolysis temperature of 1350 °C is very close to the melting point of the silicon wafer, which weakens the bonding force between the Al_2O_3 thin layer and the silicon wafer. The released reactive atoms react with the pyrolysis byproduct gas (CO and SiO_X) of the PCS, the available bonds are directed toward the surface, and the diffused Al atoms form a Si-O-Al amorphous layer. This amorphous layer plays the role of adsorbent of reactive gases and promotes the formation of SiC nanowires with a certain crystal orientation. During the growth of SiC nanowires, the oxygen and aluminum atoms in Si-O-Al may be expelled by silicon atoms, which diffuse to the edges of the crystal and form a amorphous protective shell, which also guides the growth direction of the nanowires. Therefore, the atomic content of oxygen in the pearl-shaped amorphous layer is as high as 63.39%. Overall, the highly reactive Si-O-Al layer on the top of the SiC nanowire acts as a collector of gaseous Si-C, whereas the amorphous layer on the side of the nanowire

prevents the increase of the nanowire diameter. It is assumed that the twin defects of SiC nanowires are one of the driving forces of the growth along one direction. The existing twin dislocations in the growth direction and the formation of facets with low surface energy can also improve growth rate of nanowires along the (111) crystal plane. Twin steps are more likely to adsorb atoms. When the rate of amorphous adsorption in the reaction system is greater than the crystallization rate of SiC, the pearl-like amorphous clusters appear on the nanowires, forming the pearl-chain nanowires.

Representative HRTEM images of N3 sample are depicted in Fig. 6.

It can be observed from Fig. 6(a) that the Ni catalyst is placed on the top of the SiC nanowires, indicating that N1, N2, and N3 have grown according to the VLS mechanism. The Ni catalyst controlls the growth of SiC nanowires in the (111) direction. As shown, the average diameter of nanowires is 50 nm (Fig. 6(b)). Many twin defects can be observed inside the nanowires, and a periodic sawtooth-shaped crystal structure of the SiC nanowires is noticed on the surface. As can be seen from the elemental analysis in Table 3, the catalyst droplet mainly contains 77.76% Ni and a small amount of Si, C and O. The elemental composition of single crystal nanowires is mainly Si and C with atomic ratios close to 1:1, and O with 2.38%. The amorphous layer coated on the surface of nanowires is mainly C. The SAED pattern illustrated in the inset of Fig. 6(b) shows a single crystal lattice while the lines in the middle of the lattice are attributed to the twin defects in the nanowires. The high-resolution image in Fig. 6(c) shows that the diameter of the Ni catalyst droplet is about 200 nm. The surface of the droplet is covered by an amorphous layer of Si-O-C with a thickness of 5 nm. The EDS spectrum of N3 shows that the catalyst droplets on the top of the nanowires are composed of Si, C, O, and Ni, whereas the Si-O-C mainly exists on the surface of the catalyst droplet (Fig. 6(d)).

Fig. 7 briefly illustrates the growth of SiC nanowires supported with Ni catalyst via the VLS mechanism.

As the increase of substrate temperature, Ni first forms small droplets on the substrate surface, followed by the formation of a liquid-solid interface. Subsequently, the by-product gas formed during PCS pyrolysis is continuously adsorbed on the liquid-solid interface and promotes the crystallization of Si-O-C amorphous phase. The extra unreacted C is coated on the surface of nanowires, resulting in the formation of SiC single crystal nanowires. In addition, the lowest surface-energy (111) growth is allowed. Under these conditions, the increase in nanowires diameter is limited and the single-crystal SiC nanowires are produced.

Table 3
Elemental analysis of different regions in N3 corresponding to Fig. 6(a)-(b)

Element	Si	C	O	Ni
Atomic fraction (%)				
Area 1	12.91	7.79	1.54	77.76
Area 2	49.05	48.57	2.38	–
Area 3	11.68	79.43	8.89	–

(3) Photoluminescence properties

Fig. 8 illustrates the photoluminescence spectra of A3 and N3 samples.

As shown in Fig. 8, the photoluminescent spectra at 350 nm of A3 and N3 display two obvious emission peaks at ~ 395 and 465 nm, corresponding to 3.13 and 2.67 eV, respectively. This indicates that the prepared 3C-SiC nanowires emit within a wide range of wavelengths. Yet, the intensity of the emission peaks varies according to the catalyst type. It is obvious that the morphology and structural defects influences the photoluminescence characteristics of nano-SiC crystals[12]. Herein, the shape of the emission peaks is largely similar, and the center position of the emission peak changes minimally. However, compared to the conventional SiC crystal with a relatively larger grain size for which the emission occurs at 556 nm, a significant blue shift is noticed for both samples. This can be explained by a quantum size effect, which causes the shift of the emission peak, as previously observed [13]. Among them, the presence of amorphous phase in A3 also can cause the blue shift in the center position of the emission peak.

(4) Thermal stability

The TG and DSC curves of A3 and N3 are displayed in Fig. 9.

The TG curves show no change before 1100 °C. However, above 1100 °C, a weight gain is observed for both samples, indicating that the SiC nanowire sample is further oxidized. The oxidation is more evident for the A3 sample, of which the residual mass is 105.54% (Fig. 9(a)). In this case, the sample contains Al with a lower melting point (660 °C), while the content of amorphous Si-O-Al is high and easily oxidized, which is reflected by the weight gain. N3 samples showed a relatively low rate of mass change. This is because the excess carbon in the PCS precursor is consumed by the trace of oxygen, forming a thin amorphous layer of carbon on the surface of the nanowire[14]. It can be observed from the TEM image that there is an amorphous carbon layer on the surface of SiC nanowires, and the oxidation of the amorphous carbon layer will consume and result in weight loss. Meanwhile, the weight gain and mass cancellation of the amorphous grains and Si-O-C occur during the oxidation process. N3 shows

absorption peaks at 566.69 °C, while the adsorption peak of A3 appears at 654.40 °C (Fig. 9(b)). In addition, a peak appears at 1170.36 °C,

4. Conclusions

1. SiC nanowires with pearl-chain-like morphology were prepared using Al_2O_3 as catalyst. Straight SiC nanowires were prepared with Ni as catalyst. The crystallinity of pearl-chain-like nanowires is slightly higher than that of straight nanowires. The results showed that the efficiency of the nanowires formation depends on the thickness of the catalyst film. Moreover, for the both SiC nanowires samples, the generation of twin structural defects was noticed.
2. The main mechanism governing the formation of SiC nanowires in the presence of Al_2O_3 is the OAG mechanism. In this case, the growth of nanowires is mainly controlled by the amorphous Si-O-Al coated on the surface of the nanowires while the pearl-like beads are generated due to the twin defects. The SiC nanowires grown in the presence of Ni catalyst follow the VLS mechanism. As the temperature increases, and in the presence of the catalyst, the crystallization of SiC is favored, generating the final nanowire structure.
3. SiC nanowire samples prepare with two different catalysts have emissions peaks in visible range at 395 and 465 nm. The emission peakis blue shifted in comparison with the conventional microsize SiC due to the nanosized dimension of the SiC nanowires, twin defects, and amorphous phases are identified in the samples.
4. The two samples have good thermal stability under 1000℃ in air atmosphere. Beyond this temperature, the mass of the material begins to change as a result of some slight oxidation of the material.

Declarations

Acknowledgements

This work was supported by the National Natural Science Foundation of China (Grant No. 51632007, 51602258, 51872229, 51521061), the 111 Project of China (B08040),National Science and Technology Major Project(2017-Ⅱ-0007-0077).

References

1. Zhang H, Ding W, He K*, et al.* Synthesis and Characterization of Crystalline Silicon Carbide Nanoribbons. *Nanoscale Research Letters*[J], 2010, 5(8): 1264-1271.
2. Li S, Wang N, Zhao H*, et al.* Synthesis and electrical properties of p-type 3C-SiC nanowires. *Materials Letters*[J], 2014, 126: 217-219.
3. Wang H, Lun L, Yang W*, et al.* Preferred Orientation of SiC Nanowires Induced by Substrates. *J.phys.chem.c*[J], 2012, 114(6): 2591-2594.

4. Yang G Z, Cui H, Sun Y*, et al.* Simple Catalyst-Free Method to the Synthesis of beta-SiC Nanowires and Their Field Emission Properties. *Journal Of Physical Chemistry C*[J], 2009, 113(36): 15969-15973.
5. Prakash J, Dasgupta K, Tripathi B M*, et al.* A new approach to fabricate SiC nanowire-embedded dense SiC matrix/carbon fiber composite. *Journal Of Materials Science*[J], 2014, 49(19): 6784-6792.
6. Zhu S M, Xi H A, Li Q*, et al.* In situ growth of beta-SiC nanowires in porous SiC ceramics. *Journal Of the American Ceramic Society*[J], 2005, 88(9): 2619-2621.
7. Pan J-m, Yan X-h, Cheng X-n*, et al.* Preparation of SiC nanowires-filled cellular SiCO ceramics from polymeric precursor. *Ceramics International*[J], 2012, 38(8): 6823-6829.
8. Makeev M A, Srivastava D, Menon M. Silicon carbide nanowires under external loads: An atomistic simulation study. *Physical Review B*[J], 2006, 74(16):
9. Zhang R Q, Lifshitz Y, Lee S T. Oxide-Assisted Growth of Semiconducting Nanowires. 2010, 15(7-8): 635-640.
10. Kang J H, Krizek F, Zaluska-Kotur M*, et al.* Au-Assisted Substrate-Faceting for Inclined Nanowire Growth. *Nano Lett*[J], 2018, 18(7): 4115-4122.
11. Zhang X, Chen Y, Xie Z*, et al.* Shape and Doping Enhanced Field Emission Properties of Quasialigned 3C-SiC Nanowires. *Journal Of Physical Chemistry C*[J], 2010, 114(18): 8251-8255.
12. Yu Z, Jian L, Harmer M P*, et al.* An Order–Disorder Transition in Surface Complexions and Its Influence on Crystal Growth of Boron-Rich Nanostructures. *Crystal Growth & Design*[J], 2015, 15(8): 150702135137006.
13. Yu Z, Xin F, Yuan J*, et al.* Correlating Growth Habit of Boron-Rich Low-Dimensional Materials with Defect Structures by Electron Microscopy. *Crystal Growth & Design*[J], 2013, 13(6): 2269-2276.
14. Song Q, Yan H, Liu K*, et al.* Vertically Grown Edge-Rich Graphene Nanosheets for Spatial Control of Li Nucleation. *Advanced Energy Materials*[J], 2018, 8(22):

Figures

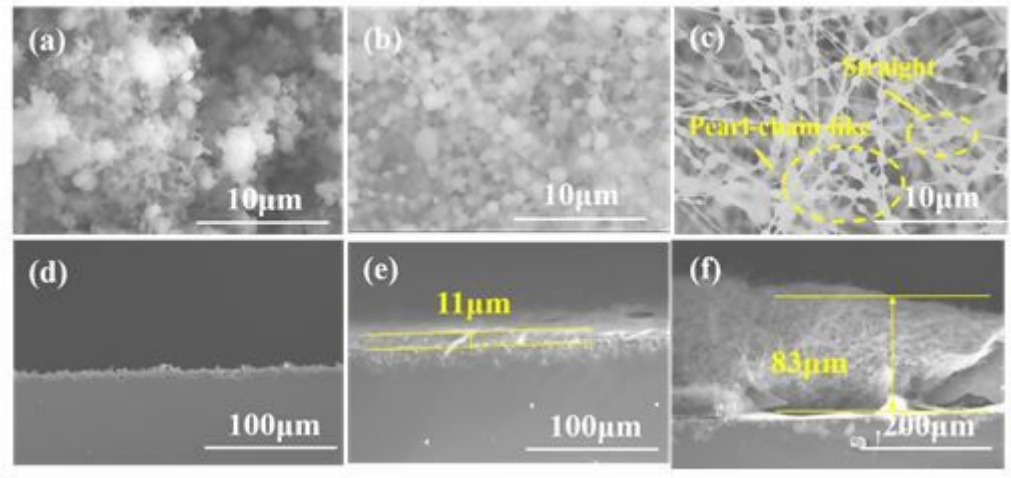

Figure 1

Surface morphology SEM images of (a) A1, (b) A2, (c) A3 SiC nanowires, Cross-section morphology SEM images of (d) A1, (e) A2, (f) A3 SiC nanowires.

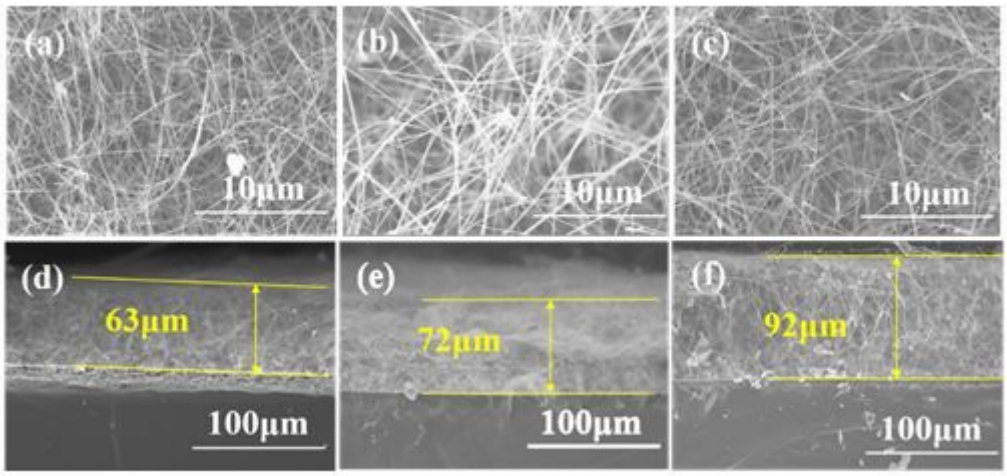

Figure 2

Surface morphology SEM images of (a) N1, (b) N2, (c)N3 SiC nanowires, Cross-section morphology SEM images of (d) N1, (e) N2, (f) N3 SiC nanowires.

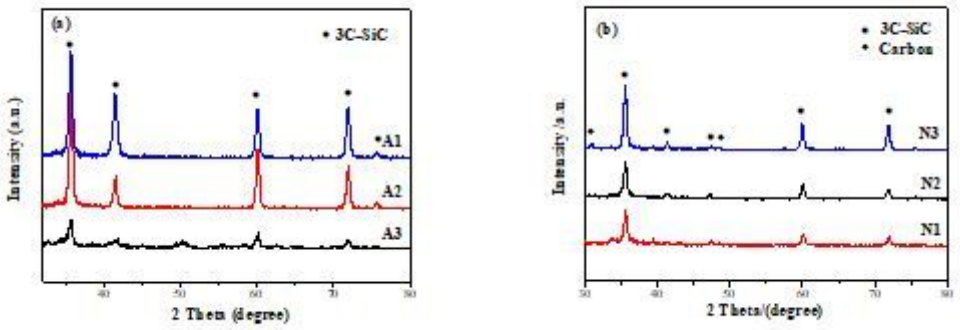

Figure 3

XRD patterns of SiC nanowires prepared with (a) Al2O3, (b) Ni catalysts.

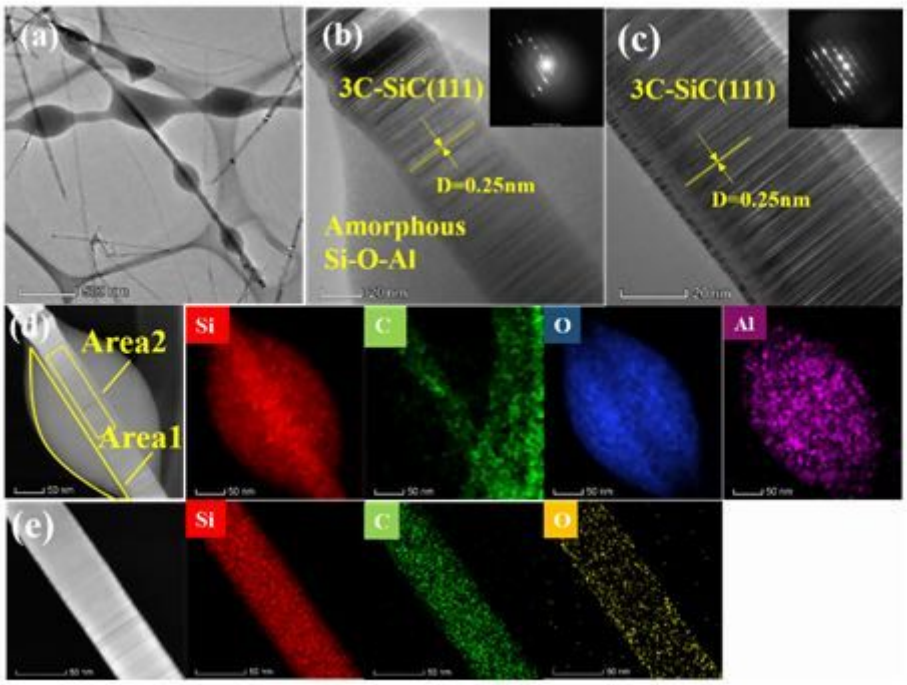

Figure 4

(a) TEM image of A3 sample, (b) HRTEM image and SAED pattern of pearl-chain-like nanowire, (c) HRTEM image and SAED pattern of straight nanowire. (d) EDS mapping of pearl-chain-like nanowire; (e) EDS mapping of straight nanowire.

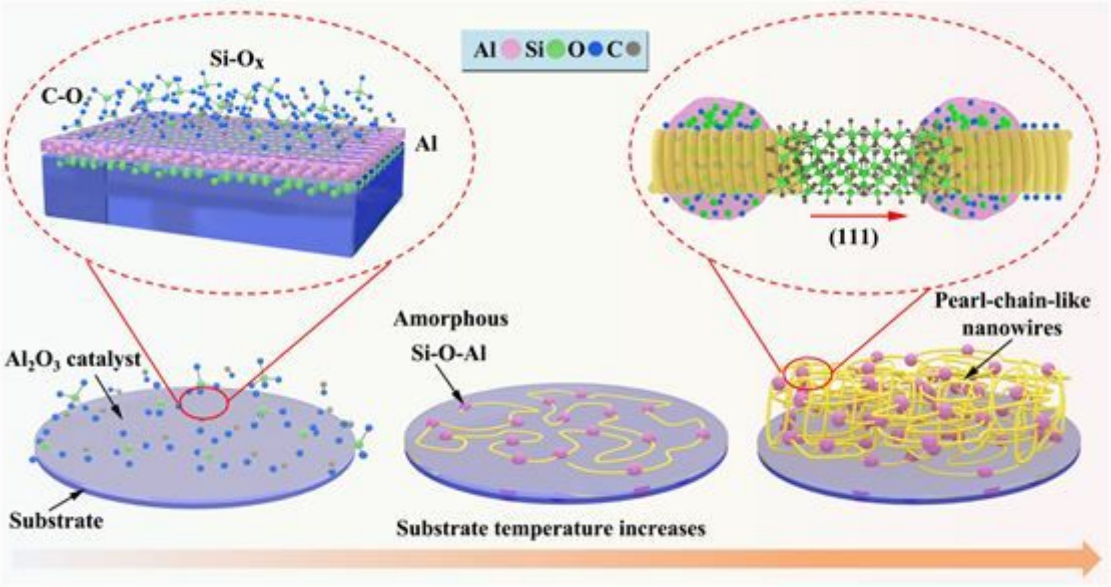

Figure 5

Schematic diagram of growth mechanisms of SiC nanowires loaded with Al2O3 catalysts.

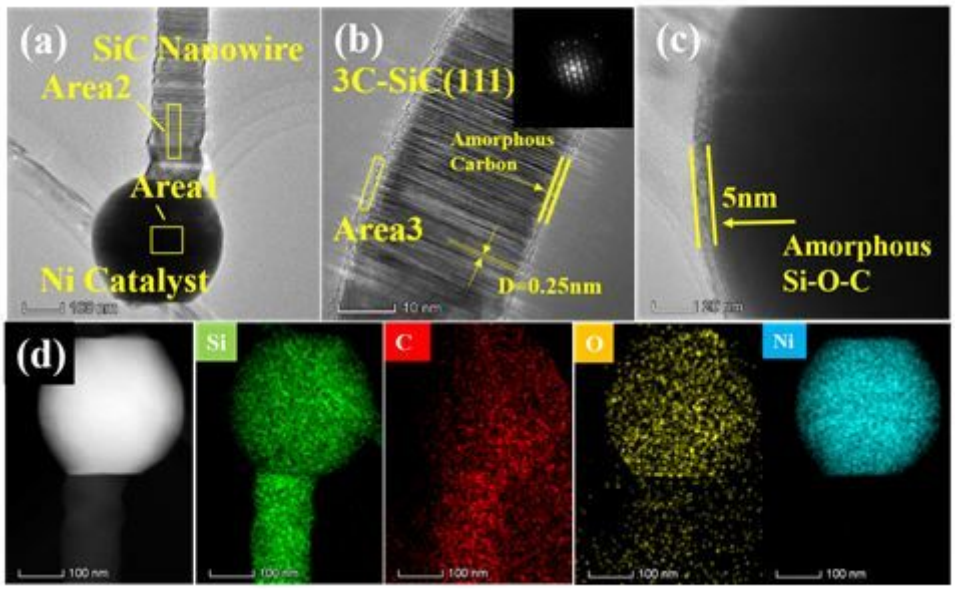

Figure 6

(a) TEM image of N3 sample. (b) HRTEM image and SAED pattern of nanowire; (c) HRTEM image of catalyst; (d) EDS mappings of N3 sample.

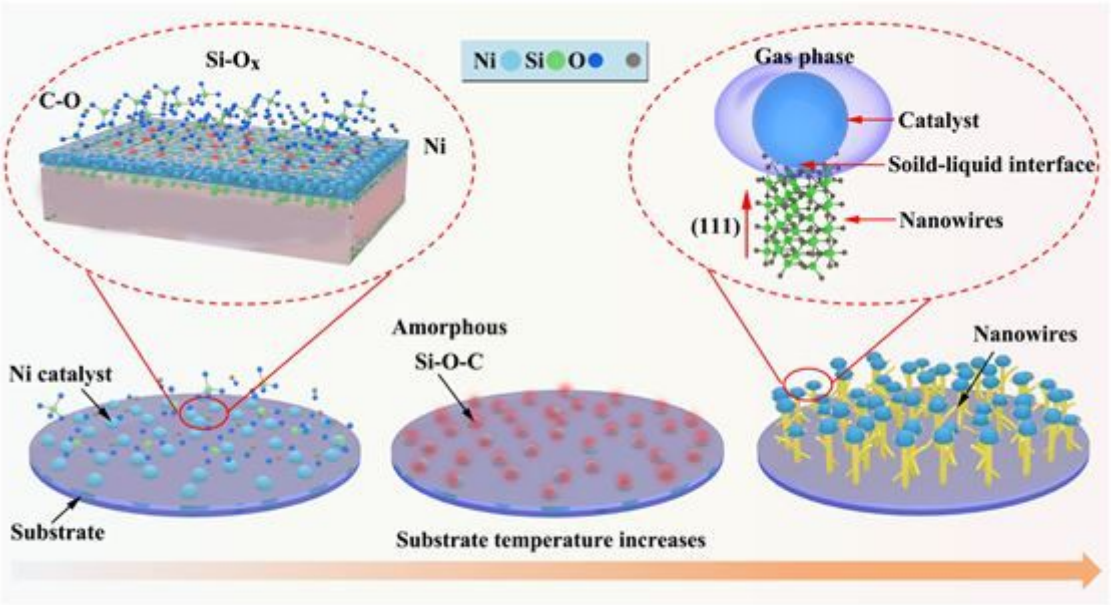

Figure 7

Schematic diagram of growth mechanisms of SiC nanowires loaded with Ni catalysts.

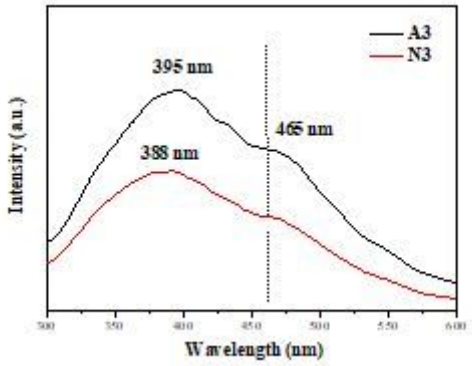

Figure 8

Photoluminescence spectra of A3 and N3 samples.

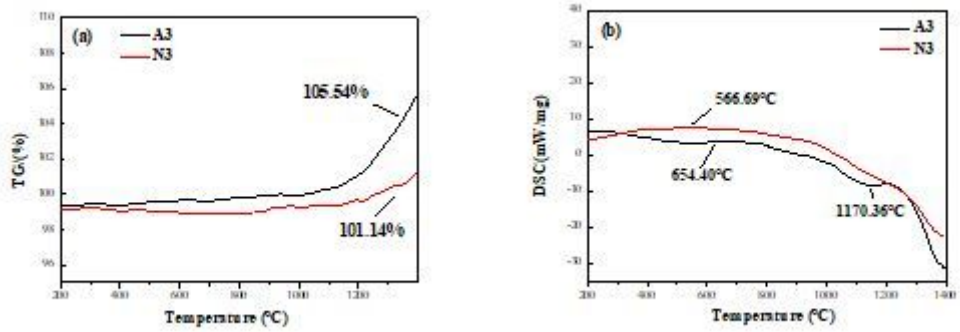

Figure 9

(a) TG and (b) DSC curves of A3 and N3 samples.